Mon. Not. R. Astron. Soc. **383,** 691–704 (2008) doi:10.1111/j.1365-2966.2007.12578.x

Reionization bias in high-redshift quasar near-zones

J. Stuart B. Wyithe,[1⋆] James S. Bolton[2] and Martin G. Haehnelt[3]

[1]*School of Physics, University of Melbourne, Parkville, Victoria, Australia*
[2]*Max-Planck-Institut fur Astrophysik, Karl-Schwarzschild Str. 1, 85748 Garching, Germany*
[3]*Institute of Astronomy, University of Cambridge, Madingley Road, Cambridge CB3 0HA*

Accepted 2007 October 11. Received 2007 October 4; in original form 2007 August 13

ABSTRACT

Absorption spectra of high-redshift quasars exhibit an increasingly thick Lyα forest, suggesting that the fraction of neutral hydrogen in the intergalactic medium (IGM) is increasing towards $z \sim 6$. However, the interpretation of these spectra is complicated by the fact that the Lyα optical depth is already large for neutral hydrogen fractions in excess of 10^{-4}, and also because quasars are expected to reside in dense regions of the IGM. We present a model for the evolution of the ionization state of the IGM which is applicable to the dense, biased regions around high-redshift quasars as well as more typical regions in the IGM. We employ a cold dark matter based model in which the ionizing photons for reionization are produced by star formation in dark matter haloes spanning a wide range of masses, combined with numerical radiative transfer simulations which model the resulting opacity distribution in quasar absorption spectra. With an appropriate choice for the parameter which controls the star formation efficiency, our model is able to simultaneously reproduce the observed Lyα forest opacity at $4 < z < 6$, the ionizing photon mean-free-path at $z \sim 4$ and the rapid evolution of highly ionized near-zone sizes around high-redshift quasars at $5.8 < z < 6.4$. In our model, reionization extends over a wide redshift range, starting at $z \gtrsim 10$ and completing as H II regions overlap at $z \sim 6$–7. We find that within 5 physical Mpc of a high-redshift quasar, the evolution of the ionization state of the IGM precedes that in more typical regions by around 0.3 redshift units. More importantly, when combined with the rapid increase in the ionizing photon mean-free-path expected shortly after overlap, this offset results in an ionizing background near the quasar which exceeds the value in the rest of the IGM by a factor of $\sim$2–3. We further find that in the post-overlap phase of reionization the size of the observed quasar near-zones is not directly sensitive to the neutral hydrogen fraction of the IGM. Instead, these sizes probe the level of the background ionization rate and the temperature of the surrounding IGM. The observed rapid evolution of the quasar near-zone sizes at $5.8 < z < 6.4$ can thus be explained by the rapid evolution of the ionizing background, which in our model is caused by the completion of overlap at the end of reionization by $6 \lesssim z \lesssim 7$.

Key words: galaxies: formation – intergalactic medium – cosmology: theory.

1 INTRODUCTION

The reionization of cosmic hydrogen, which is commonly believed to have been due to ultraviolet photons produced by the first stars and quasars (Barkana & Loeb 2001), was an important milestone in the history of the Universe. The recent discovery of very distant quasars has enabled detailed studies of the ionization state of the high-redshift intergalactic medium (IGM) to be made at a time when the universe was less than a billion years old (White et al. 2003; Fan et al. 2006). Several studies have used the evolution of the ionizing background inferred from these spectra to argue that the reionization of cosmic hydrogen was completed just beyond $z \sim 6$ (White et al. 2003; Fan et al. 2006; Gnedin & Fan 2006). However, other authors have claimed that the evidence for this rapid change becomes significantly weaker for a different choice density distribution in the IGM (Becker, Rauch & Sargent 2007). One reason for the ambiguity in interpreting these absorption spectra is that Lyα absorption can only be used to probe neutral fractions that are larger than 10^{-4}, owing to the large cross-section of the Lyα resonance.

Several of the most-distant quasars exhibit complete Gunn–Peterson (GP) troughs, the red edges of which do not extend as

⋆E-mail: swyithe@physics.unimelb.edu.au

far as the redshifted Lyα wavelength. A possible interpretation of the observation of a GP trough which does not extend all the way to the Lyα wavelength is the presence of an H II region in a partially neutral IGM (e.g. Cen & Haiman 2000; Madau & Rees 2000). This interpretation has been used in different ways to argue that there is a significant fraction of neutral hydrogen in the IGM beyond $z \sim 6$ (Mesinger & Haiman 2004; Wyithe & Loeb 2004; Wyithe, Loeb & Carilli 2005), with a lower limit on the hydrogen neutral fraction that is as much as two orders of magnitude larger than constraints available from direct absorption studies. Bolton & Haehnelt (2007a), Maselli et al. (2007) and Lidz et al. (2007), however, have argued that this interpretation is uncertain and that these observed regions of transmission could be either due to an H II region or due to a classical proximity zone.

Given this uncertainty, and in order to connect the evolution of the IGM ionization state at redshifts both above and below those where the GP troughs have been observed, Fan et al. (2006) proposed defining the sizes of these regions of transmission as the distance where the smoothed spectrum first drops below the level where 10 per cent of the flux is transmitted. Bolton & Haehnelt (2007a) refer to this region as the highly ionized near-zone, and Fan et al. (2006) argued that its size should reflect the ionization state of the IGM in a simple way. Using this definition, Fan et al. (2006) found a rapid trend of near-zone size with redshift, from which they inferred an order of magnitude increase in the neutral fraction of the IGM over the observed range of $5.8 \lesssim z \lesssim 6.4$. However, Bolton & Haehnelt (2007a) demonstrated that the near-zone size becomes independent of the neutral hydrogen fraction when the IGM is highly ionized.

In this paper, we will address two points regarding the interpretation of the near-zones observed in high-redshift quasar absorption spectra. As pointed out recently by Lidz et al. (2007) and Alvarez & Abel (2007), the quasars observed prior to $z \sim 6$ are likely to have formed in regions substantially pre-ionized by nearby clustered galaxies. We therefore first discuss the extent to which regions of the IGM observed close to high-redshift quasars in absorption spectra are representative of the Universe on average, using a density-dependent semi-analytic model for the re-ionization history. This model is carefully calibrated to be consistent with the current observational data, and as such provides a consistent theoretical framework for modelling quasar near-zones in highly biased regions of the IGM. We then use this model to predict the sizes of quasar near-zones and their evolution with redshift, both semi-analytically and using detailed simulations of radiative transfer.

We begin by describing our density-dependent semi-analytic model for the reionization history (Section 2), including our procedures for the calculation of the ionizing background. We then present results for the bias of re-ionization near quasars in Section 3, before discussing the evolution of the observed high-redshift quasar near-zones using the semi-analytic model in Section 4. We then explore this model in more detail with full radiative transfer simulations in Section 5. We present our conclusions in Section 6. Throughout this paper, we adopt the set of cosmological parameters determined by *WMAP* (Spergel et al. 2007) for a flat Λ cold dark matter (ΛCDM) universe, namely $\Omega_{\rm m} = 0.24, \Omega_\Lambda = 0.76$ and $h = 0.73$. In computation of the mass function, we assume a primordial power spectrum defined by a power law with index $n = 0.95$, an exact transfer function given by Bardeen et al. (1986) and rms mass density fluctuations with a sphere of radius $R_8 = 8h^{-1}$ Mpc of $\sigma_8 = 0.76$.

2 SEMI-ANALYTIC MODEL FOR RE-IONIZATION

Miralda-Escudé et al. (2000) presented a model which allows the calculation of an effective recombination rate in an inhomogeneous universe by assuming a maximum overdensity ($\Delta_{\rm c}$) which may be penetrated by ionizing photons within H II regions. The model assumes that reionization progresses rapidly through islands of lower density prior to the overlap of individual ionized regions. Following overlap, the remaining regions of high density are gradually ionized. It is therefore hypothesized that at any time, regions with gas below some critical normalized density threshold $\Delta_{\rm i} \equiv \rho_i/\langle\rho\rangle$ are ionized while regions of higher density are not. In what follows, we draw primarily from their prescription and refer the reader to the original paper for a detailed discussion of its motivations and assumptions. Wyithe & Loeb (2003) employed this prescription within a semi-analytic model of reionization. In this work, we limit our attention to reionization due to Population II stars (Gnedin & Fan 2006; Srbinovsky & Wyithe 2007), which govern the final stages of reionization even in the presence of an earlier partial or full reionization by Population III stars (e.g. Wyithe & Loeb 2003). We do not consider quasars in our analysis. While quasars dominate the ionizing background at lower redshifts, they have been shown not to contribute to the ionizing background at $z \sim 6$, or to provide a contribution comparable to that of stars until $z \lesssim 4$ (Srbinovsky & Wyithe 2007). Moreover, should there be a quasar contribution to the ionizing background, this will be included implicitly as stellar radiation, since in this paper we match our model to the observed level of ionizing background radiation.

Within the model of Miralda-Escudé et al. (2000), we describe the post-overlap evolution of the IGM by computing the evolution of $\mathrm{d}F_{\rm M}(\Delta_{\rm i})/\mathrm{d}z$, where

$$F_{\rm M}(\Delta_{\rm i}) = \int_0^{\Delta_{\rm i}} \mathrm{d}\Delta\, P_{\rm V}(\Delta)\Delta \tag{1}$$

is the fraction of mass in regions with overdensity below $\Delta_{\rm i}$, and $P_{\rm V}(\Delta)$ is the volume-weighted probability distribution for Δ. In a region of large-scale overdensity δ at $z_{\rm obs}$, the mass fraction $F_{\rm M}(\Delta_{\rm i})$ (or equivalently $\Delta_{\rm i}$) therefore evolves according to the equation

$$\frac{\mathrm{d}F_{\rm M}(\Delta_{\rm i})}{\mathrm{d}z} = \frac{1}{n_0\left[1+\delta\frac{D(z)}{D(z_{\rm obs})}\right]}\frac{\mathrm{d}n_\gamma(\delta)}{\mathrm{d}z} - \alpha_{\rm B}\frac{R(\Delta_{\rm i})}{a^3}n_0\left[1+\delta\frac{D(z)}{D(z_{\rm obs})}\right]\frac{\mathrm{d}t}{\mathrm{d}z}, \tag{2}$$

where D is the growth factor, $\alpha_{\rm B}$ is the case B recombination coefficient, n_0 is the comoving density of hydrogen in the mean IGM, and $R(\Delta_{\rm i})$ is the effective clumping factor of the IGM (see below). The evolution is driven by the rate of emission of ionizing photons per comoving volume $\mathrm{d}n_\gamma(\delta)/\mathrm{d}z$, which is discussed in Section 2.2. This equation was described in Wyithe & Loeb (2003), but it is generalized in this work to apply to regions of large-scale overdensity δ that differ from the average IGM.

Integration of equation (2) requires knowledge of $P_{\rm V}(\Delta)$. Miralda-Escudé et al. (2000) found that a good fit to the volume-weighted probability distribution for the density as seen in cosmological hydrodynamic simulations has the functional form

$$P_{\rm V}(\Delta)\mathrm{d}\Delta = A\exp\left[-\frac{(\Delta^{-2/3}-C_0)^2}{2(2\delta_0/3)^2}\right]\Delta^{-\beta}\mathrm{d}\Delta, \tag{3}$$

with $\delta_0 = 7.61/(1+z)$ and $\beta = 2.23$, 2.35 and 2.48, and $C_0 = 0.558$, 0.599 and 0.611 at $z = 2$, 3 and 4. At $z = 6$, they assume $\beta = 2.5$ and solve for A and C_0 by requiring the mass and volume to be normalized to unity. We repeat this procedure to find $P_{\rm V}(\Delta)$ at higher redshifts. The proportionality of δ_0 to the scalefactor is expected for the growth of structure in an $\Omega_{\rm m} = 1$ universe or at high redshift otherwise, and its amplitude should depend on the amplitude of the power spectrum. The simulations on which the distribution in Miralda-Escudé et al. (2000) was based assumed $\Omega_{\rm m} = 0.4, \Omega_\Lambda = 0.6$ and $\sigma_8 = 0.79$, close to the values used in this paper. The above probability distribution remains a reasonable description at high redshift when confronted with a more modern cosmology and updated simulations, although the addition of an analytical approximation for the high-density tail of the distribution remains necessary as a best guess at correcting for numerical resolution (Bolton & Haehnelt 2007b).

Equation (2) provides a good description of the evolution of the ionization fraction following the overlap of individual ionized bubbles because the ionization fronts are exposed to the mean ionizing radiation field. However, prior to overlap, the prescription is inadequate due to the large fluctuations in the intensity of the ionizing radiation. A more accurate model to describe the evolution of the ionized volume prior to overlap was suggested by Miralda-Escudé et al. (2000). In our notation, the appropriate equation is

$$\frac{{\rm d}[Q_{\rm i} F_{\rm M}(\Delta_{\rm c})]}{{\rm d}z} = \frac{1}{n_0 \left[1+\delta\frac{D(z)}{D(z_{\rm obs})}\right]} \frac{{\rm d}n_\gamma(\delta)}{{\rm d}z} - \alpha_{\rm B}(1+z)^3 R(\Delta_{\rm c}) n_0 \left[1+\delta\frac{D(z)}{D(z_{\rm obs})}\right] Q_{\rm i} \frac{{\rm d}t}{{\rm d}z}. \quad (4)$$

or

$$\frac{{\rm d}Q_{\rm i}}{{\rm d}z} = \frac{1}{n_0 \left[1+\delta\frac{D(z)}{D(z_{\rm obs})}\right] F_{\rm M}(\Delta_{\rm c})} \frac{{\rm d}n_\gamma(\delta)}{{\rm d}z} - \left\{ \alpha_{\rm B}(1+z)^3 R(\Delta_{\rm c}) n_0 \left[1+\delta\frac{D(z)}{D(z_{\rm obs})}\right] \frac{{\rm d}t}{{\rm d}z} + \frac{{\rm d}F_{\rm M}(\Delta_{\rm c})}{{\rm d}z} \right\} \frac{Q_{\rm i}}{F_{\rm M}(\Delta_{\rm c})}. \quad (5)$$

In this expression, $Q_{\rm i}$ is redefined to be the volume filling factor within which all matter at densities below $\Delta_{\rm c}$ has been ionized. The effective clumping of the IGM can now be written as

$$R(\Delta_{\rm i}) \equiv Q_{\rm i} \frac{\langle\rho^2\rangle}{\langle\rho\rangle^2} = \int_0^{\Delta_{\rm i}} {\rm d}\Delta P_{\rm V}(\Delta)\Delta^2. \quad (6)$$

Within this formalism, the epoch of overlap is precisely defined as the time when $Q_{\rm i}$ reaches unity. However, we have only a single equation to describe the evolution of two independent quantities $Q_{\rm i}$ and $F_{\rm M}$. The relative growth of these depends on the luminosity function and spatial distribution of the sources. The appropriate value of $\Delta_{\rm c}$ is set by the mean separation of the ionizing photon sources. More numerous sources can attain overlap for smaller values of $\Delta_{\rm c}$. We assume $\Delta_{\rm c}$ to be constant with redshift before overlapping with values of $\Delta_{\rm c} = 20$ and $\Delta_{\rm c} = 5$ (which lie in the range for galaxies) in this paper, and show examples for both.

Our approach is to compute a reionization history, given a particular value of $\Delta_{\rm c}$, combined with assumed values for the efficiency of star formation and the fraction of ionizing photons that escape from galaxies. With this history in place, we then compute the evolution of the background radiation field due to these same sources. Post-overlap, ionizing photons will experience attenuation due to residual overdense pockets of H I gas. We use the description of Miralda-Escudé et al. (2000) to estimate the ionizing photon mean-free-path, and subsequently derive the attenuation of ionizing photons. We then compute the flux at the *Lyman limit* ($\nu_{\rm L} = 3.29 \times 10^{15}$ Hz) in the IGM due to sources immediate to each epoch, in addition to redshifted contributions from earlier epochs. This calculation follows the model described in Srbinovsky & Wyithe (2007) (see also Choudhury & Ferrara 2005) but is summarized below.

We note that H I Lyman limit photons (13.6 eV) are incapable of ionizing helium (He) [24.6 eV (He II), 54.4 eV (He III)]. We therefore neglect He when computing the intensity of the ionizing background in our semi-analytic model.

2.1 Evaluating flux at the Lyman limit

In this section, we review the process for calculating the ionizing background flux at a particular redshift. We assume the post-overlap ionizing background to be generated by Population II stars alone following the results of Srbinovsky & Wyithe (2007). We first define z_0 to be the redshift at which the flux is to be evaluated. The flux at the Lyman limit is normalized in *physical* units of $J_{21}(10^{-21}\,{\rm erg\,s^{-1}\,Hz^{-1}\,cm^{-2}\,sr^{-1}})$, and at redshift z_0 it is related to the energy density by

$$J_{21}(z_0) = \frac{c}{4\pi} \frac{{\rm d}^2 E^{\rm tot}_{\nu_{\rm L}}(z_0)}{{\rm d}V{\rm d}\nu} \frac{1}{10^{-21}} (1+z_0)^3, \quad (7)$$

where c is the speed of light and $\frac{{\rm d}^2 E^{\rm tot}_{\nu_{\rm L}}(z_0)}{{\rm d}V{\rm d}\nu}$ is the energy per unit frequency interval per unit comoving volume at frequency $\nu_{\rm L}$ and redshift z_0. Contributions to the radiation field at $\nu_{\rm L}$ (and z_0) from sources at redshift z were emitted at frequency $\nu_z = \frac{1+z}{1+z_0}\,\nu_{\rm L}$. Note that ν_z remains below the He Lyman limit (24.6 eV) whilst $\frac{1+z}{1+z_0} \lesssim 2$. The semi-analytic model of the re-ionization history predicts an average redshift of overlap, which we refer to as $z_{\rm ol}$.

The ionizing background flux contains contributions from sources at z_0 in addition to redshifted flux from sources at higher redshift. To compute the ionizing background flux, we consider contributions from sources with redshifts $z > z_0$. The total comoving energy density at redshift z_0 is

$$\frac{{\rm d}^2 E^{\rm tot}_{\nu_{\rm L}}(z_0)}{{\rm d}V{\rm d}\nu} = \int_\infty^{z_0} {\rm d}z \frac{{\rm d}^3 E_{\nu_z}(z)}{{\rm d}V{\rm d}\nu{\rm d}t} Q_{\rm i} \left(\frac{1+z_0}{1+z}\right)^3 {\rm e}^{-\tau(z,z_0)} \frac{{\rm d}t}{{\rm d}z}. \quad (8)$$

The term $\frac{{\rm d}^3 E_{\nu_z}(z)}{{\rm d}V{\rm d}\nu{\rm d}t}$ represents the frequency-dependent (comoving) energy density per unit time generated by ionizing sources, and τ is the optical depth for ionizing photons between z and z_0. Rather than assuming the complete attenuation of ionizing photons emitted prior to the redshift of overlap, we instead assume attenuation due to the mean-free-path evaluated in ionized regions prior to overlap and weigh the contribution to the energy density by $Q_{\rm i}$. This approach should approximate the contribution of sources to the ionizing background that emit at redshifts late in the overlap epoch when the typical bubble size is evolving rapidly, and is much larger than the ionizing photon mean-free-path (Furlanetto, Zaldarriaga & Hernquist 2004).

Finally, the photoionization rate may be related to the observed ionizing background flux using

$$\Gamma = 4\pi \int_{\nu_{\rm L}}^\infty \frac{J_\nu}{h_{\rm p}\nu} \sigma_\nu {\rm d}\nu, \quad (9)$$

where σ_ν is the H I photoionization *cross-section* and $h_{\rm p}$ is Planck constant. Using equation (9) and the spectra describing our sources,

we find[1] $\Gamma_{12} = 2.82 J_{21}$ (where Γ_{12} is the ionizing rate in units of 10^{-12} s^{-1}) for a background in which stars are the dominant source. This last step does not account for the variation in the spectral shape (due to redshifting) from that emitted at a constant time.

2.2 Lyman limit photons from stars

We next describe the contribution to the ionizing background flux made by Population II stars. To begin, we describe the spectral energy distribution (SED) of Population II star-forming galaxies, using the model presented in Leitherer et al. (1999). The SED has the form $\frac{\mathrm{d}^3 E_\nu}{\mathrm{d}\nu\,\mathrm{d}t\,\mathrm{d}\dot{M}}$, where $\dot{M}$ is expressed in units of (baryonic) solar masses per year. In the instance that ionizing photons are produced primarily in starbursts, with lifetimes much shorter than the Hubble time, we may express the star formation rate per unit time as

$$\frac{\mathrm{d}\dot{M}}{\mathrm{d}V}(z) = f^* \frac{\mathrm{d}F(\delta, z)}{\mathrm{d}t_{\rm year}} \rho_{\rm b}, \tag{10}$$

where $\rho_{\rm b}$ is the comoving baryonic mass density, and $F(\delta, z)$ is the density-dependent collapsed fraction of mass in haloes above a critical mass at z. The factor f^* (the star formation efficiency) describes the fraction of collapsed matter that participates in star formation. This fraction is largely unknown.

In a region of comoving radius R and mean overdensity $\delta(z) = \delta D(z)/D(z_{\rm obs})$ (specified at redshift z instead of the usual $z = 0$), the relevant collapsed fraction is obtained from the extended Press & Schechter (1974) model (Bond et al. 1991) as

$$F(\delta, R, z) = \mathrm{erfc}\left(\frac{\delta_{\rm c} - \delta(z)}{\sqrt{2\left([\sigma_{\rm gal}]^2 - [\sigma(R)]^2\right)}}\right), \tag{11}$$

where $\mathrm{erfc}(x)$ is the error function, $\sigma(R)$ is the variance of the density field smoothed on a scale R, and $\sigma_{\rm gal}$ is the variance of the density field smoothed on a scale $R_{\rm gal}$, corresponding to a mass scale of $M_{\rm min}$ or $M_{\rm ion}$ (both evaluated at redshift z rather than at $z = 0$). In this expression, the critical linear overdensity for the collapse of a spherical top-hat density perturbation is $\delta_c \approx 1.69$.

In a cold neutral IGM beyond the redshift of reionization, the collapsed fraction should be computed for haloes of sufficient mass to initiate star formation. The critical virial temperature is set by the temperature ($T_{\rm N} \sim 10^4$ K) above which efficient atomic hydrogen cooling promotes star formation. Following the re-ionization of a region, the Jeans mass in the heated IGM limits accretion to haloes above $T_{\rm I} \sim 10^5$ K (Efstathiou 1992; Thoul & Weinberg 1996; Dijkstra et al. 2004). We may therefore write the time-derivative of the collapsed fraction as

$$\frac{\mathrm{d}F}{\mathrm{d}t_{\rm year}}(z) = \left[Q_{\rm m}(z)\frac{\mathrm{d}F(z, T_{\rm I})}{\mathrm{d}z} + [1 - Q_{\rm m}(z)]\frac{\mathrm{d}F(z, T_{\rm N})}{\mathrm{d}z}\right] \times \frac{\mathrm{d}z}{\mathrm{d}t_{\rm year}}, \tag{12}$$

where $Q_{\rm m}$ is the ionized mass fraction in the universe.

To describe the ionizing flux from stars, we require one further parameter. Only a fraction of ionizing photons produced by stars may enter the IGM. Therefore, an additional factor of $f_{\rm esc}$ (the escape fraction) must be included when computing the emissivity due to stars. Ciardi & Ferrara (2005) include a review of existing constraints on $f_{\rm esc}$ which suggests that its value is $\lesssim$15 per cent. The star formation efficiency and escape fraction may be combined into a single free parameter ($f^*_{\rm esc}$) to describe the contribution of stars in our model. The energy density due to Population II stars at z_0 may be computed using equation (8) with $\frac{\mathrm{d}^3 E_{\nu_z}(z)}{\mathrm{d}V\,\mathrm{d}\nu\,\mathrm{d}t}$ given by

$$\frac{\mathrm{d}^3 E_{\nu_z}(z)}{\mathrm{d}V\,\mathrm{d}\nu\,\mathrm{d}t} = \frac{\mathrm{d}^3 E_{\nu_z}(z)}{\mathrm{d}\nu\mathrm{d}t\mathrm{d}\dot{M}} \frac{\mathrm{d}F(z)}{\mathrm{d}t_{\rm year}} \rho_{\rm b} f^*_{\rm esc}. \tag{13}$$

This energy density may then be converted to a flux.

Finally, the quantity $\frac{\mathrm{d}F}{\mathrm{d}t_{\rm year}}(z)$ may also be used to estimate the rate of emission of ionizing photons per comoving volume which is required to compute the re-ionization history equations (2)–(5):

$$\frac{\mathrm{d}n_\gamma(\delta)}{\mathrm{d}z} = N_\gamma f^*_{\rm esc} \frac{\mathrm{d}F}{\mathrm{d}z} n_0 \left[1 + \delta \frac{D(z)}{D(z_{\rm obs})}\right], \tag{14}$$

where N_γ is the number of ionizing photons produced per baryon incorporated into stars. We find $N_\gamma = 4200$ for the stellar spectra adopted in this paper. Note that $\mathrm{d}n_\gamma(\delta)/\mathrm{d}z$ is computed using a collapsed fraction that is dependent on the local overdensity, and therefore includes the effects of galaxy bias.

2.3 Attenuation of ionizing photons

Having computed a luminosity density, we may now compute a value for the ionizing background using equations (7)–(9), following the calculation of the optical depth (τ). We fix $\Delta_{\rm c}$ prior to overlap, and then follow the evolution of $\Delta_{\rm i}$ following overlap. In each case, we use the approach of Miralda-Escudé et al. (2000) to estimate the mean-free-path (λ) as a function of redshift (z_i):

$$\lambda_i = \lambda_0 (1 - F_{\rm v})^{-2/3}. \tag{15}$$

Here

$$F_{\rm v} = \int_0^{\Delta_{\rm max}(z)} \mathrm{d}\Delta P(\Delta) \tag{16}$$

is the volume filling factor of ionized regions, computed using the the volume-weighted probability distribution [$P(\Delta)$] of the overdensity (Miralda-Escudé et al. 2000), and $\Delta_{\rm max}$ is equal to $\Delta_{\rm c}$ and $\Delta_{\rm i}$ prior to and following overlap, respectively. We note that prior to overlap the mean-free-path is ill-defined, and we calculate the mean-free-path for photons in *ionized regions* prior to overlap. The product $\lambda_0 H = 60\,\mathrm{km\,s^{-1}}$ was obtained from comparison to the scales of Lyα forest structures in simulations, at $z = 3$ (Miralda-Escudé et al. 2000). Finally, the mean-free-path as a function of redshift may be used to compute the attenuation of ionizing photons between redshifts z and z_0. The resulting optical depth is

$$\tau(z, z_0) = \int_z^{z_0} \mathrm{d}z \frac{c\mathrm{d}t}{\mathrm{d}z} \frac{1}{\lambda_i}. \tag{17}$$

2.4 The overdensity near massive haloes

Strong clustering of massive sources implies that these sources should trace the higher density regions of IGM. In this section, we compute the distribution of overdensities on a scale R that are centered on haloes of mass M. Our aim is to calculate the distribution of overdensities surrounding high-redshift quasars, which are expected to be larger compared to an average region of the IGM (e.g. Faucher-Giguere et al. 2007; Guimarães et al. 2007).

The likelihood of observing a galaxy at a random location is proportional to the number density of galaxies. At small values of the large-scale overdensity δ, this density is proportional to

[1] This conversion was reported incorrectly in Srbinovsky & Wyithe (2007) as $\Gamma_{12} = 1.69 J_{21}$.

$[1 + \delta b(M, z)]$, where b is the galaxy bias (Mo & White 1996; Sheth, Mo & Tormen 2001). More generally, given a large-scale overdensity δ on a scale R, the likelihood of observing a galaxy may be estimated[2] from the Sheth & Tormen (2002) mass function as

$$\mathcal{L}_{\rm g}(\delta) = \frac{(1+\delta)\nu(1+\nu^{-2p})\mathrm{e}^{-a\nu^2/2}}{\bar{\nu}(1+\bar{\nu}^{-2p})\mathrm{e}^{-a\bar{\nu}^2/2}}, \quad (18)$$

where $\nu = (\delta_{\rm c} - \delta)/[\sigma(M)]$ and $\bar{\nu} = \delta_{\rm c}/[\sigma(M)]$. Here $\sigma(M)$ is the variance of the density field smoothed with a top-hat window on a mass scale M at redshift z, and $a = 0.707$ and $p = 0.3$ are constants. Note that here as elsewhere in this paper, we work with overdensities and variances computed at the redshift of interest (i.e. not extrapolated to $z = 0$). Utilizing Bayes theorem, we find the a posteriori probability distribution for the overdensity δ on the scale R, given the locations defined by a galaxy population. We obtain

$$\left.\frac{\mathrm{d}P}{\mathrm{d}\delta}\right|_{\rm gal} \propto \mathcal{L}_{\rm g}(\delta)\frac{\mathrm{d}P_{\rm prior}}{\mathrm{d}\delta}, \quad (19)$$

where $\frac{\mathrm{d}P_{\rm prior}}{\mathrm{d}\delta}$ is the prior probability distribution for δ, which is described by a Gaussian of variance $\sigma(R)$. We may use this probability for the overdensity within R of a luminous high-redshift quasar to calculate the enhancement in the recombination and star formation rates. Thus, through integration of equations (2) and (5), we may compute the reionization history within typical regions surrounding luminous quasars, and compare these with the reionization history of the mean IGM ($\delta = 0$).

3 RESULTS

The model described in the previous section has two free parameters $\Delta_{\rm c}$ and $f^*_{\rm esc}$. For any combination of these parameters, we are able to compute a reionization history, the evolution of the mean-free-path, and the evolution of the ionizing background as a function of the local overdensity. In this section, we first summarize the observations to which we compare our model before describing the results of this comparison.

3.1 Observational estimates of the ionization rate

Fan et al. (2006) have analysed the absorption spectra of 19 high-redshift quasars. Based on these data, Bolton & Haehnelt (2007b) present estimates of the ionization rate, Γ_{12} and the neutral hydrogen fraction over a range of redshifts near the end of the reionization era using a suite of detailed numerical simulations. In Figs 1 and 2, we compare our model to these estimates to demonstrate that it is consistent with the available data.

3.2 Comparison of reionization near a quasar and in the general IGM

We now use the model developed earlier to address the level of bias in reionization near a luminous high-redshift quasar relative to the IGM as a whole. We show results for a particular model in which we assume that quasars are hosted by haloes of mass $10^{13}\,{\rm M}_\odot$ for $\Delta_{\rm c} = 20$. Although we compare our model for the ionizing background to only three observational points at $z \gtrsim 4$ using two free parameters, $\Delta_{\rm c}$ and $f^*_{\rm esc}$, we find that these parameters are not degenerate following overlap. Larger values of $\Delta_{\rm c}$ increase the volume of hydrogen that must be reionized prior to overlap, leading to a delay in the reionization redshift. However, following overlap, the mean-free-path increases rapidly, and hence Γ_{12} at redshifts below $\sim$5 is quite insensitive to $\Delta_{\rm c}$. On the other hand, varying $f^*_{\rm esc}$ strongly affects the overlap redshift, since the critical number of ionizing photons per baryon is achieved earlier. Following overlap, a larger $f^*_{\rm esc}$ also increases the value of Γ_{12}, which is proportional to the local emissivity in addition to the mean-free-path. We therefore adjust the parameter $f^*_{\rm esc}$ so that the model evaluated at the mean density of the Universe gives a good fit to the observed ionizing background (we find $f^*_{\rm esc} = 0.0037$). The best fit to the ionization rate observed at $z \sim 6$ is provided by a value of $\Delta_{\rm c} \sim 20$. Values of $\Delta_{\rm c} \gtrsim 5$ also yield a satisfactory fit. The overlap redshifts corresponding to $(\Delta_{\rm c}, f^*_{\rm esc}) =$ (20, 0.0037) and (5, 0.0037) are $z_{\rm ol} = 6.2$ and 7.2, respectively.

This model generates an optical depth to Thomson scattering for CMB photons of $\tau_{\rm es} = 0.45$, which is smaller than the values determined from the *WMAP* satellite ($\tau_{\rm es} = 0.089 \pm 0.03$), though only at the 1.5σ level (Spergel et al. 2007). Models which include the possible effect of massive Population III stars partially reionize the IGM at higher redshifts and result in larger values of $\tau_{\rm es}$. For example, in the work of Choudhury & Ferrara (2006) and Wyithe & Cen (2007), models in which the reionization history shows an extended plateau of mostly ionized IGM in the range $6 \lesssim z \lesssim 10$ are able to produce values of $\tau_{\rm es}$ within the preferred range plus completion of reionization at $z \sim 6$. We ignore a possible early component of reionization in this paper since we find that it would have limited effect on the evolution of the ionizing background during the completion of overlap at $z \sim 6$.

We note that the value of $f_{\star,{\rm esc}}$ required for our model to reproduce existing observations is in good agreement with external considerations. In particular, our value of $f_{\star,{\rm esc}}$ approximately a few times 10^{-3} corresponds to the product of recent estimates for the escape fraction (a few times 10^{-2}; Gnedin, Kravtsov & Chen 2007), with estimates of the average star formation rate ($\sim 10^{-1}$ from the ratio between the mass density in stars and baryons; Fukugita, Hogan & Peebles 1998).

Fig. 1 shows the redshift evolution of $Q_{\rm i}$, $\lambda_{\rm i}$, the volume-averaged neutral fraction and the ionization rate for the best-fitting model. Reionization histories for four different values of overdensity were computed. These overdensities were evaluated in 5 physical Mpc spheres, and correspond, respectively, to the mean overdensity centered on a quasar at $z \sim 6$ (dark solid lines) and to the $\pm 1\sigma$ fluctuations around that mean (dotted and dashed lines). We also show the case of the mean IGM with $\delta = 0$ (thick grey lines). The examples demonstrate the level of enhancement in the reionization process within 5 physical Mpc of a high-redshift quasar, and the expected scatter around this enhancement.

In the top left-hand panel of Fig. 1, we show the fraction of the IGM yet to overlap according to the definition given in Section 2. The more overdense regions experience overlap first due to the enhanced production of ionizing photons in these regions. In this model, the mean IGM achieves overlap at $z \sim 6.1$. However, within 5 physical Mpc of a quasar the overlap is achieved $\sim$0.25 redshift units earlier on average, with a 1σ scatter of $\sim$0.2 redshift units. These results are in quantitative agreement with the analytic calculation of Lidz et al. (2007, see their fig. 1). However, our model allows the

[2] We note that we have used the Press & Schechter (1974) mass function to estimate the production of ionizing photons within biased regions of the IGM, but the Sheth & Tormen (2002) formalism to estimate clustering of massive galaxies. This approach is not self-consistent, but is sufficient for our purposes since the ionizing photon production is dominated by low-mass galaxies whose density is described within the Press–Schechter formalism, while the Sheth–Tormen model more accurately estimates the statistics of massive galaxies.

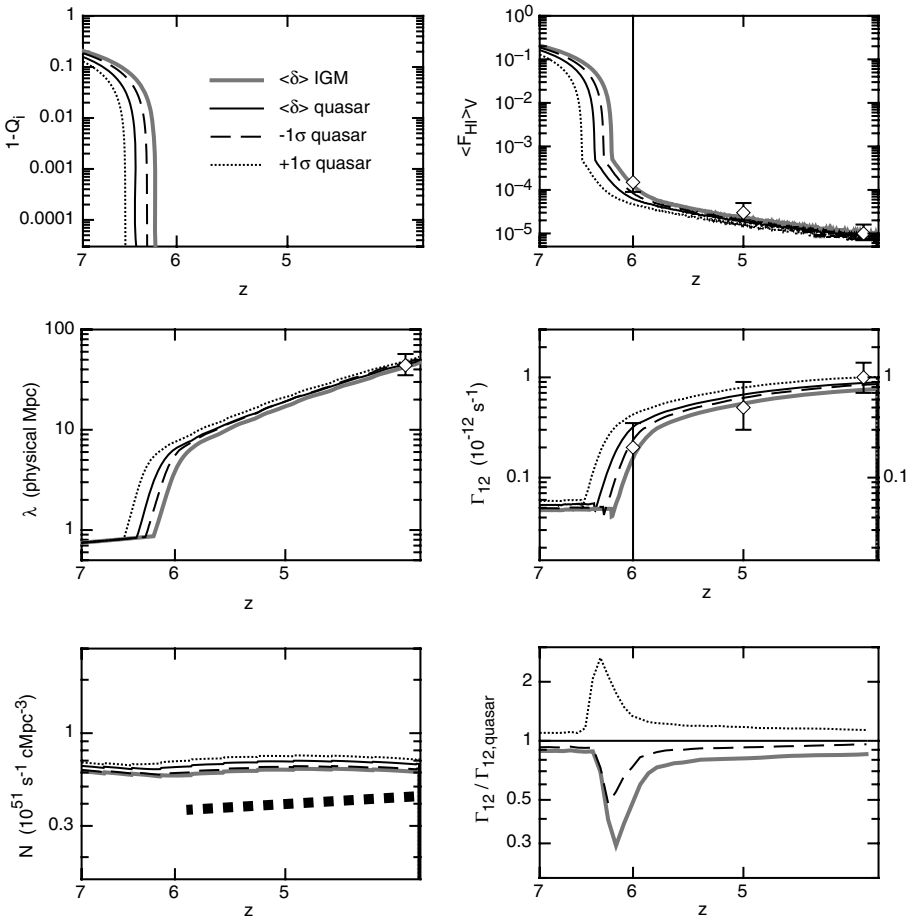

Figure 1. The effect of overdensity on the redshift of overlap, and the subsequent ionization state of the IGM. Four cases are shown, corresponding to different overdensities evaluated in 5 physical Mpc spheres, including the average overdensity centred on a quasar at $z \sim 6$ (dark solid curves) and the $\pm 1\sigma$ fluctuations around that mean (dotted and dashed curves). We also show the case of the mean IGM with $\delta = 0$ (thick grey lines). Top left-hand panel: the fraction of the IGM yet to overlap according to the definition of overlap given in Section 2. Top right-hand panel: the volume-averaged filling factor of neutral gas. Central left-hand panel: the mean-free-path for ionizing photons computed using the formalism in Section 2. Central right-hand panel: the ionization rate. Lower left-hand panel: the emissivity of ionizing sources. Also shown (thick dotted line) is the observed evolution of ionizing sources as estimated in Bolton & Haehnelt (2007b). Lower right-hand panel: the ratio of the ionization rate at different overdensities relative to the average overdensity centred on a quasar host. In this example, the halo mass was $M = 10^{13}\,\mathrm{M}_{\odot}$ and $\Delta_c = 20$. The observational points in the top and middle right-hand panels are also from Bolton & Haehnelt (2007b).

calculation of post-overlap properties such as the volume-averaged neutral fraction, ionizing photon mean-free-path and ionization rate in addition to the pre-overlap mass-averaged ionization fraction.

In the central left-hand panel of Fig. 1, we show the corresponding value of the mean-free-path for ionizing photons, computed using the formalism in Section 2. The model predicts a rapid increase in the mean-free-path following overlap, which is also indicated from the results of numerical simulations, (e.g. Gnedin 2000). However, the offset in the overlap redshift induced by large-scale overdensity leads to substantial differences in mean-free-path within regions of different average overdensities for a brief period following overlap. Once the rate of change of mean-free-path slows, then its dependence on overdensity is reduced.

In the central right-hand panel of Fig. 1, we show the dependence of the ionization rate on redshift. The rapid change in the mean-free-path following overlap leads to a corresponding rapid change in the ionization rate. Thus, for a brief period near overlap the model predicts large variations in the ionizing background within regions with different mean overdensities. Note that the rapid increase in Γ_{12} is entirely due to the increasing mean-free-path, and not to an increase in the source emissivity which is shown in the lower left-hand panel of Fig. 1. Indeed, the radiative feedback that accompanies the end of the reionization era results in a slight reduction in the emissivity during the time when the ionizing background undergoes a large increase. For comparison, the fit to the observationally derived ionizing emissivity from Bolton & Haehnelt (2007b) is shown by the thick dotted line. The model emissivity is close to the observationally derived estimate (with the offset due to the assumption of a somewhat harder spectrum here), and it has a similar (small) redshift dependence. In the upper right-hand panel, we show the volume-averaged hydrogen neutral fraction. Again, near overlap the value of the neutral fraction inferred within the vicinity of high-redshift quasars is significantly biased relative to the average IGM. To better illustrate the level and duration of the bias introduced by early overlap, we also plot the ionization rate at different overdensities relative to the average overdensity centred on a quasar host halo (lower right-hand panel of Fig. 1). We see that at times near overlap, the ionizing background within 5 physical Mpc of a quasar can be as much as a factor of 3 in excess of the average ionizing background. We have also checked the enhancement of the ionizing background

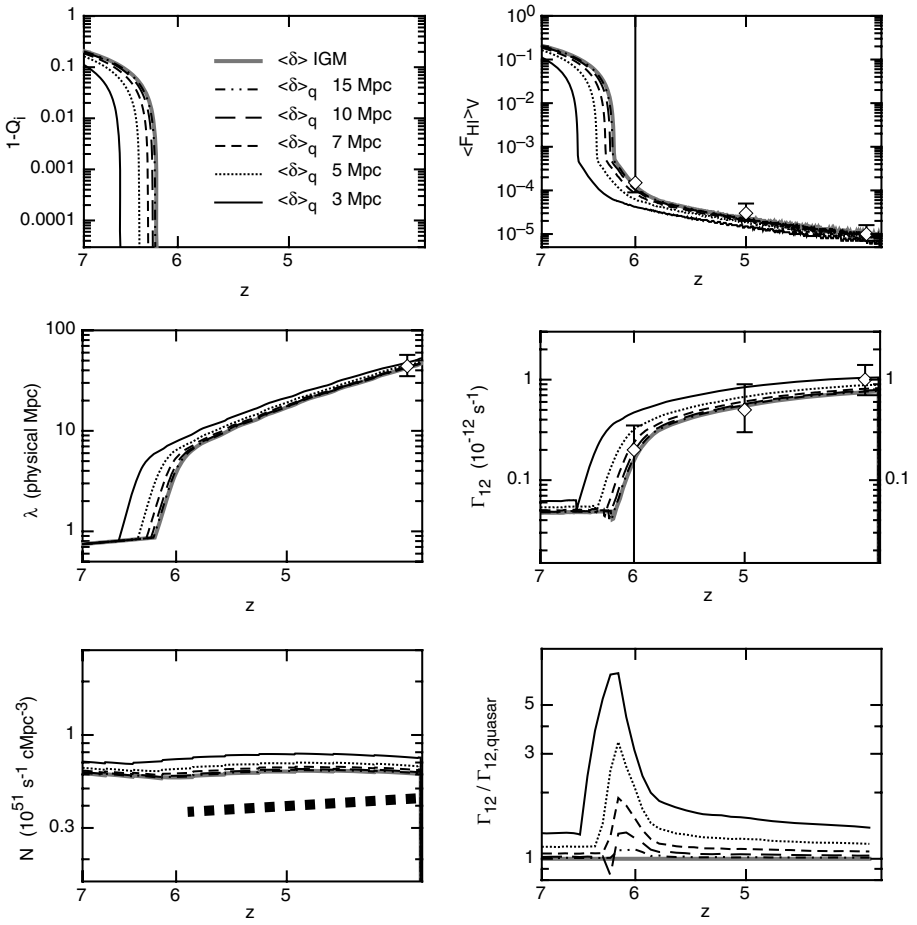

Figure 2. The effect of overdensity on the redshift of overlap, and the subsequent ionization state of the IGM. Five cases are shown, corresponding to overdensities evaluated within spheres with radii between 5 and 15 physical Mpc, centred on a quasar at $z \sim 6$. In each case, we evaluate the reionization history assuming the mean overdensity surrounding the quasar. We also show the case of the mean IGM with $\delta = 0$ (thick grey lines). Top left-hand panel: the fraction of the IGM yet to overlap according to the definition of overlap given in Section 2. Top right-hand panel: the volume-averaged filling factor of neutral gas. Central left-hand panel: the mean-free-path for ionizing photons computed using the formalism in Section 2. Central right-hand panel: the ionization rate. Lower left-hand panel: the emissivity of ionizing sources. Also shown (thick dotted line) is the observed evolution of ionizing sources summarized in Bolton & Haehnelt (2007b). Lower right-hand panel: the ratio of the ionization rate at different overdensities relative to the average overdensity centred on a quasar host. In this example, the halo mass was $M = 10^{13}\,\mathrm{M}_{\odot}$ and $\Delta_c = 20$. The observational points in the top and middle right-hand panels are also from Bolton & Haehnelt (2007b).

(at a fixed distance) near a quasar host following overlap for different values of the quasar host mass and Δ_c. We find that the enhancement is reduced for smaller values of the quasar host mass, but is not sensitive to the value of the critical overdensity Δ_c.

3.3 The dependence of re-ionization on the distance from a quasar

In the previous section, we saw that the early reionization of overdense regions will lead to an ionizing background within 5 physical Mpc of a high-redshift quasar that is in excess of the average IGM by a factor of $\sim$3. In this section, we explore the variation in this enhancement with distance from the quasar. As before, in Fig. 2 we plot the effect of overdensity on the redshift of overlap, and the subsequent ionization state of the IGM. We again assume the case of $\Delta_c = 20$ and a quasar host mass of $10^{13}\,\mathrm{M}_{\odot}$. Five cases are shown, corresponding to overdensities evaluated within spheres with radii between 5 and 15 physical Mpc, centred on a quasar at $z \sim 6$. In each case, we evaluate the history assuming the mean overdensity surrounding the quasar host of mass $M = 10^{13}\,\mathrm{M}_{\odot}$. We also show the case of the mean IGM with $\delta = 0$ (thick grey lines).

In the top left-hand panel of Fig. 2, we show the fraction of the IGM that has yet to overlap. Re-ionization will occur earlier in regions that are closer to the quasar, where the overdensity is typically higher. In the central left-hand panel, we plot the mean-free-path for ionizing photons. At a fixed time around overlap, we expect that the mean-free-path will be larger closer to the quasar. It is important to note that throughout the epoch where the evolution of the mean-free-path is rapid, the mean-free-path is smaller than the distances from the quasar under consideration. This condition is required for our model to be applicable, since otherwise it would overestimate the ionizing background within the region. In the upper right-hand and central right-hand panels, we plot the volume-averaged neutral fraction of hydrogen and the ionization rate. As before we also plot the model and observed emissivity of ionizing sources in the lower left-hand panel. Finally, in the lower right-hand panel we show the ratio of the average ionization rate within different radii relative to the the value calculated at the average overdensity centred on

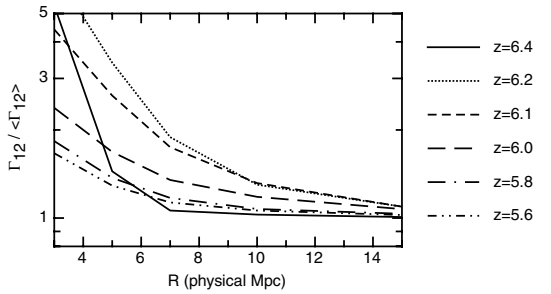

Figure 3. The ratio of ionization rates due to galaxies calculated at the mean overdensity found within spheres of radius R surrounding a high-redshift quasar, relative to the ionization rate in the mean IGM. The curves are plotted over a range of redshifts between $z = 5.6$ and 6.4. The overlap of the mean IGM in this model (with $\Delta_c = 20$) is at $z = 6.2$. The quasar host masses were $10^{13}\,M_\odot$.

a quasar host. As expected, we find that the level of enhancement decreases as the distance from the quasar increases.

To better see the dependence of the ionization rate on radius, we plot its enhancement within a spherical region of radius R surrounding a quasar relative to the mean IGM (Fig. 3). The values are shown for a range of redshift bins near overlap. The enhancement in the ionizing background is greatest close to the quasar, where the overdensity is largest. We find that the enhancement drops below 10 per cent beyond distances of 15 physical Mpc. At all scales, the enhancement is largest at a time shortly after the overlap of the average IGM. The enhancement more than halves in value by around half a redshift unit after overlap, and has almost disappeared by 1 redshift unit following overlap.

Before proceeding we note that we have not included the effect of the quasar in our calculation of the enhancement of the ionizing background near the quasar. The additional ionizing flux from the quasar would increase the local value of the ionizing photon mean-free-path, and therefore increase the value of the ionization rate due to the stellar emissivity. The enhancements described in Fig. 2 should therefore be considered as lower limits.

4 THE EVOLUTION OF QUASAR NEAR-ZONES

We now turn to the prediction of Lyα near-zone sizes. Bolton & Haehnelt (2007a), Maselli et al. (2007) and Lidz et al. (2007) have shown that the interpretation of near-zone sizes with respect to the neutral hydrogen fraction in the IGM is difficult. Indeed, the data may approximately correspond to the edge of an H II region surrounded by a neutral IGM or instead correspond to a classical proximity zone in a highly ionized IGM. As discussed in the Introduction section, Fan et al. (2006) proposed defining the sizes of these regions of transmission as the distance where the smoothed spectrum first drops below the level where 10 per cent of the flux is transmitted. Using this definition, Fan et al. (2006) found a rapid trend of near-zone size with redshift, from which they inferred an order of magnitude increase in the neutral fraction of the IGM over the observed range $5.8 \lesssim z \lesssim 6.4$. However, the detailed modelling of Bolton & Haehnelt (2007a) showed that the evolution of the near-zone size is not a simple function of the neutral hydrogen fraction. Their modelling suggested that in the limit of a classical proximity zone the rapid evolution of near-zone sizes could be explained by a relatively modest evolution in the neutral fraction, with the rapid evolution being due to the approach of the background transmission reaching 10 per cent.

The evolution of the ionization state of the IGM is thus difficult to extract from the observed evolution of the near-zone size. In this section, we begin by discussing a calculation of quasar near-zone sizes using our semi-analytic re-ionization model. We then describe the observed relation between near-zone size and redshift before comparing our model with the observed evolution of quasar near-zone size.

4.1 Semi-analytic estimates for the evolution of near-zone sizes

In Fig. 4, we plot the ionization rate due to galaxies in a biased, overdense region of the IGM surrounding a quasar. The ionization rates are displayed as a function of radius from the quasar. The overlap of the mean IGM in the model used (which was shown in Figs 1 and 4 and has $\Delta_c = 20$) is at $z = 6.2$. The quasar host mass is $10^{13}\,M_\odot$, and its ionizing luminosity is $\dot{N} = 2 \times 10^{57}\,s^{-1}$. In the left-hand panel, we show the ionization rate due to galaxies calculated at the mean overdensity found within spheres of radius R surrounding a high-redshift quasar. The curves are plotted at a range of redshifts between $z = 5.6$ and 6.4. The ionization rate due to the quasar emission assuming the IGM to be optically thin is also shown (thick grey line). We see that at redshifts near $z \sim 5.8$, the value of the ionization rate at distances corresponding to the observed quasar near-zone sizes ($\sim$10 Mpc) is comparable to the ionization rate due to the quasar alone. Moreover, at this epoch, the value of the galaxy ionization rate increases rapidly with redshift due to the increasing mean-free-path at the end of the overlap epoch. In the right-hand panel of Fig. 4, we show the corresponding ionization rates due to the sum of the galaxies plus the central quasar. Note that we have linearly added the ionization rates and thus do not account for the expected increase in the mean free-path due to the ionizing radiation

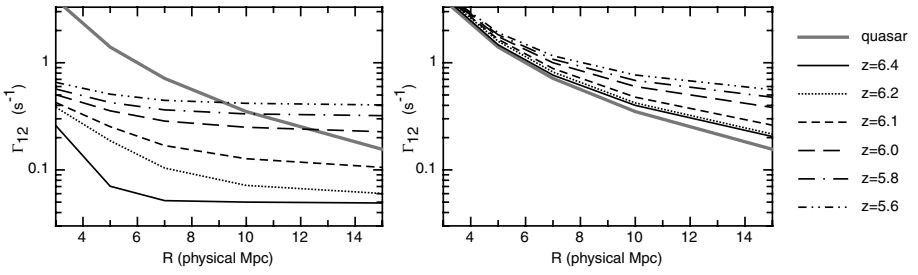

Figure 4. The ionization rate as a function of radius from a quasar. Left-hand panel: the ionization rate due to galaxies calculated at the mean overdensity found within spheres of radius R surrounding a high-redshift quasar. The curves are plotted at a range of redshifts between $z = 5.6$ and 6.4. The ionization rate due to the quasar in a highly ionized IGM is also shown (thick grey line). Right-hand panel: the corresponding ionization rates due to galaxies plus the central quasar. The overlap of the mean IGM in this model (with $\Delta_c = 20$) is at $z = 6.2$. The quasars host masses were $10^{13}\,M_\odot$, and their ionizing luminosities were $\dot{N} = 2 \times 10^{57}\,s^{-1}$.

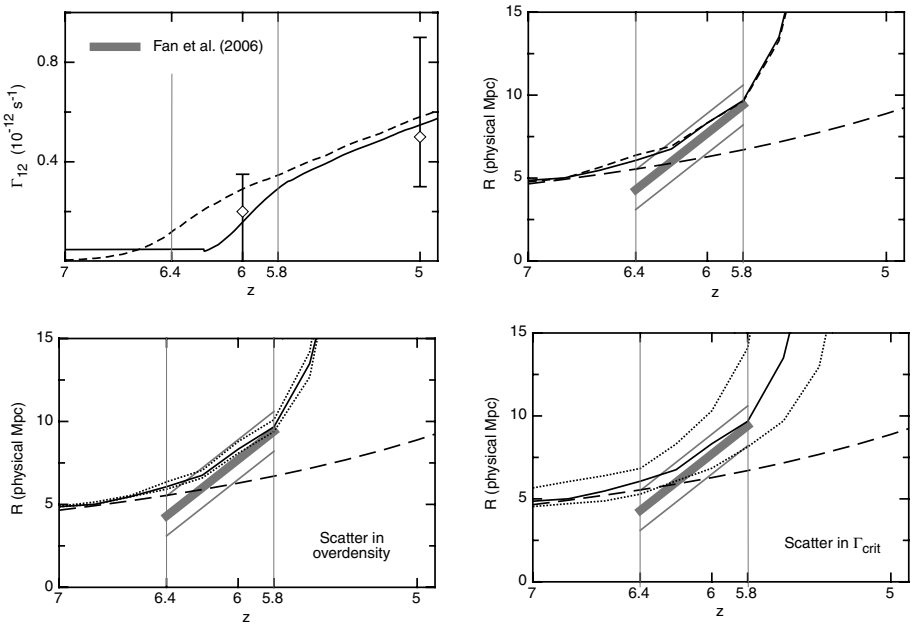

Figure 5. The predicted evolution of quasar near-zone sizes as a function of redshift. Upper left-hand panel: the evolution of the ionization rate corresponding to regions at the mean IGM density (solid line $\Delta_c = 20$; dashed line $\Delta_c = 5$). Upper right-hand panel: the predicted evolution of the near-zone size. The solid line corresponds to the size expected assuming the mean overdensity surrounding a quasar. The long-dashed line shows the near-zone evolution expected due to expansion of the Universe only. Also shown for comparison (thick grey line) is the observed near-zone size evolution, which may be parametrized by $R_{max} = 7.7$–$8.1(z - 6)$ physical Mpc (see section 4.2). The thin grey lines illustrate the level of observed scatter (± 1.2 Mpc). Lower left-hand panel: as before, except now the dotted curves correspond to the near-zone size evolution computed at -1σ and $+1\sigma$ fluctuations around the mean density for $\Delta_c = 20$. Lower right-hand panel: as before, but now the dotted lines correspond to the near-zone size evolution computed for $z_{10} = 5.0$ and 5.5, each for $\Delta_c = 20$. The overlap redshifts (with $f^*_{esc} = 0.0037$) of the mean IGM in these models are at $z = 6.2$ (with $\Delta_c = 20$) and $z = 7$ (with $\Delta_c = 5$). In all panels, the quasar host masses were assumed to be 10^{13} M$_\odot$, and quasar ionizing luminosities were $\dot{N} = 2 \times 10^{57}$ s^{-1}.

of the quasar. We therefore still underestimate the ionization rate somewhat in the quasar near-zone in our model. The contribution to the ionization rate from galaxies flattens the radial power-law profile of the ionization rate at large distances surrounding the quasar. This flattening becomes more pronounced towards lower redshifts.

We now turn to an analytical estimate of quasar near-zone sizes within our re-ionization model. Adopting the near-zone size definition of Fan et al. (2006) discussed previously, we firstly need to estimate the ionization rate which leads to a transmission level of 10 per cent. Fan et al. (2006) smoothed their spectra on a 20 Å scale to compute the near-zone size; an effective Lyα optical depth of $\tau_{eff} = -\ln(0.1) = 2.3$ is therefore an appropriate measure to estimate this quantity. The IGM exhibits an effective optical depth of 2.3 around $z_{10} \sim 5.2$ (Songaila 2004; Fan et al. 2006), at which point our semi-analytic reionization model predicts a value we will denote as $\Gamma(5.2)$. Therefore, the limiting value of the ionization rate which will correspond to a transmission level of 10 per cent at some redshift is approximately given by

$$\Gamma_{lim} = \Gamma(5.2) \left(\frac{1+z}{6.2} \right)^{9/2}, \quad (20)$$

since $\Gamma \propto (1+z)^{9/2}$ for a fixed optical depth (e.g. Bolton & Haehnelt 2007a). We may therefore estimate the near-zone size as the value of R at which the sum of the galaxy and quasar ionizing rates in Fig. 4 drops below Γ_{lim}. Note that while we are confident in our model's ability to estimate the background ionization rate, our analytic estimate of near-zone size is very approximate due to the neglect of several important effects. These effects include the attenuation of the quasars' ionizing flux in the near-zone as well as the effect of discrete absorbers on the observed near-zone size (our analytic model computes only the mean properties of a clumpy IGM). We will address these issues using a numerical model of radiative transfer through a realistic simulation of the high-redshift IGM in Section 5.

The semi-analytic predictions for the evolution of quasar near-zone sizes as a function of redshift are shown in the upper right-hand panel of Fig. 5. The redshift evolution for sizes calculated at the mean overdensity surrounding a quasar is plotted as the solid line. We show two cases, $\Delta_c = 20$ (solid line) and $\Delta_c = 5$ (dashed line). The corresponding evolution of Γ_{12} is compared to the observational data in the upper left-hand panel of Fig. 5. Fig. 5 shows that the near-zone size should not evolve much prior to the redshift of overlap where the quasar dominates the ionizing flux in the near-zone. However, when the ionization rate due to galaxies approaches the level necessary to maintain a mean transmission of 10 per cent, the near-zone size starts to evolve rapidly until eventually the definition of the near-zone size introduced by Fan et al. (2006) breaks down. This is because the flux level in most of the spectrum eventually exceeds 10 per cent, and the edge of the near-zone becomes indistinguishable from the Lyα forest.

4.2 Observations of the near-zone size

We now discuss our predictions for the near-zone size evolution in comparison with the observational data. Fan et al. (2006) found a rapid evolution in the near-zone size with redshift. Their data show a strong correlation about a mean relation, with a scatter that is in excess of the uncertainty on individual parameters. To remove the

dependence of near-zone size on quasar luminosity, L, Fan et al. (2006) rescaled their near-zone sizes to a common absolute magnitude of $M_{1450} = -27$ by assuming that the sizes are proportional to $L^{1/3}$. However, we caution that the uncertainty in the interpretation of the nature of the near-zones (H II region versus classical proximity zone) makes the scaling of the near-zone size with the ionizing luminosity of the quasar rather uncertain (Bolton & Haehnelt 2007a).

In addition to the near-zone measurements of Fan et al. (2006), Willott et al. (2007) have recently measured the near-zones for two new high-redshift quasars. In particular, they find sizes of 6.4 Mpc at $z = 6.12$, and 6.3 Mpc at $z = 6.43$. Willott et al. (2007) use the $L^{1/3}$ scaling suggested by Fan et al. (2006), and obtain revised values of 6.4 Mpc at $z = 6.12$ and 10.8 Mpc at $z = 6.43$, with the latter point in particular apparently weakening the claim for evolution of near-zone size with redshift (Willott et al. 2007). However, Willott et al. (2007) used the definition of near-zone size suggested by Bolton & Haehnelt (2007a), who defined the near-zone size to be the last pixel at which the unsmoothed quasar spectrum drops below a transmission level of 10 per cent. This definition avoids smoothing out important features in the spectrum, but breaks down once the IGM as a whole becomes highly ionized and the edge of the near-zones becomes ambiguous. Here, we use the definition of Fan et al. (2006) to facilitate a comparison with the published sizes of Fan et al. An inspection of the spectra published by Willott et al. (2007) shows that the near-zones are substantially smaller when the Fan et al. (2006) definition is employed. Therefore, our revised values for the near-zone sizes of the Willott et al. (2007) quasars are ∼4.5 Mpc at $z = 6.12$ and ∼3.5 Mpc at $z = 6.43$. Rescaling these to account for luminosity differences (using $L^{1/3}$), we find scaled values of ∼4.5 Mpc at $z = 6.12$ and ∼6 Mpc at $z = 6.43$. Thus, using a consistent near-zone definition, the near-zone sizes for the new quasars discovered by Willott et al. (2007) are consistent with the relation between near-zone size and redshift measured by Fan et al. (2006).

Following Fan et al. (2006), we quantify the evolution of the near-zone using a parametrized form for the evolution:

$$R = R_6 - \alpha(z - 6), \tag{21}$$

where R_6 is the value of the near-zone size at $z = 6$, and α is the slope of the evolution in units of Mpc. Assuming the uncertainty (σ_i) for each of the $N_q = 18$ (including both the Fan et al. 2006 and Willott et al. 2007 samples) observed near-zone sizes (R_i) at redshift z_i to be smaller than the intrinsic scatter (σ_R), we performed a χ^2 fit minimizing the variable

$$\chi^2(R_6, \alpha) = \Sigma_{i=0}^{i=N_q} \frac{[R_i - R(z_i)]^2}{\sigma_R^2}. \tag{22}$$

The intrinsic scatter is estimated by adjusting σ_R to a level that yields a minimum value of reduced χ^2 equal to unity.

The resulting constraints on α and R_6 are presented in Fig. 6 assuming scalings of $L^{1/3}$ (Fan et al. 2006) and $L^{1/2}$, as is appropriate if the near-zone is the observational signature of a classical proximity effect (Bolton & Haehnelt 2007a). The extrema of the contours shown represent the 68, 84, 91 and 97 per cent bounds on single parameters. We find values of $R_6 = 7.7 \pm 0.75$ and $\alpha = 8.1 \pm 2$ with an intrinsic scatter of $\sigma_R = 1.2$ assuming a scaling of $L^{1/2}$ and values of $R_6 = 7.9 \pm 1$ and $\alpha = 7.5 \pm 2.5$ with an intrinsic scatter of $\sigma_R = 1.5$ assuming a scaling of $L^{1/2}$. The resulting constraint on R_6 is consistent with that quoted by Fan et al. (2006). However, their quoted slope of $\alpha = 9$ was somewhat higher than our revised value, partly due to neglect of intrinsic scatter, and partly due to the addition of the two additional quasars from Willott et al. (2007).

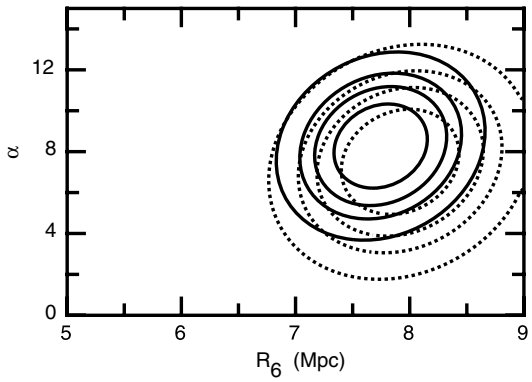

Figure 6. Constraints on the parameters α and R_6 that describe the evolution of observed near-zone sizes with redshift, assuming scalings of $L^{1/2}$ (dotted contours) and $L^{1/3}$ (solid contours), respectively. In each case, the extrema of the contours presented represent the 68, 84, 91 and 97 per cent bounds on single parameters.

In the case of a uniformly ionized IGM, Bolton & Haehnelt (2007a) have emphasized that the size of the quasar near-zone is independent of both the neutral fraction of the surrounding IGM and the quasar's lifetime, providing that the background ionization rate at the near-zone edge is small in comparison to the quasar ionization rate. The near-zone size defined in this way is plotted as the dashed line in Fig. 5 using the analytic model of Bolton & Haehnelt (2007a) (their equation 10 with $\Delta_{lim} = 0.6$). The figure shows that the evolution of near-zone size due to density evolution alone would yield a value of $\alpha = 2$, which is excluded by the data at more than 95 per cent. This disagreement implies that an additional effect is responsible for the observed evolution. As suggested by Bolton & Haehnelt (2007a), and as we will argue in more detail here using a model consistent with recent observational constraints, this additional effect is most likely due to the increasing amplitude of the ionizing background towards lower redshifts which raises the overall transmission of the IGM.

4.3 Comparison between the semi-analytic model and observations

For comparison with our semi-analytic model, we show the observed evolution of the quasar near-zones with redshift (Fig. 5; thick grey line). This evolution may be parametrized by $R_{max} = 7.7$–$8.1(z - 6)$ physical Mpc (Fig. 6). The thin lines illustrate the level of observed scatter. Both the predicted size and evolution of the quasar near-zones are similar to observations for this re-ionization model (which was not tuned beyond the requirement to fit the ionization rate at $z \sim 4$–6).

The near-zone sizes measured by Fan et al. (2006) show significant scatter, whose source we now discuss. First, while quasars are typically found in overdense regions, there are fluctuations in the overdensity of the nearby IGM, and hence also fluctuations in the stage of reionization occurring at a fixed redshift around different quasars. In the lower left-hand panel of Fig. 5, we re-plot the $\Delta_c = 20$ case for the average overdensity surrounding a quasar, and also plot the curves corresponding to the -1σ and $+1\sigma$ density fluctuations around the mean (dotted lines). Our model predicts an amount of scatter in the near-zone sizes due to this cosmic variance that is significantly smaller than the scatter in observed near-zone

sizes. The observed scatter is therefore due to the differing properties of the density field along different quasar lines-of-sight as has been shown previously in numerical simulations (Bolton & Haehnelt 2007a; Lidz et al. 2007; Maselli et al. 2007). The variation among lines-of-sight, which must be described by a full numerical treatment, is manifested as scatter in the value of ionization rate that allows a transmission of 10 per cent. We may therefore estimate the scatter in the near-zone size using our analytic model by computing the dependence of near-zone size on redshift over the range of z_{10} allowed by observation. This is shown in the lower right-hand panel of Fig. 5, again for the $\Delta_c = 20$ case, with the mean shown by the solid line and the evolution for $z_{10} = 5.0$ and 5.5 shown by the dotted lines. The scatter introduced is comparable to that of the observations. (Note that we do not expect additional scatter from quasar luminosity which has been scaled out in the relation of Fan et al. 2006, or from quasar lifetime which does not effect the size of the near zone in a highly ionized IGM Bolton & Haehnelt 2007a.) There may, however, be additional scatter due to variations in the temperature of the surrounding IGM attributable to the temperature dependence of the recombination coefficient.

Finally, it is important to note that the qualitative behaviour of the near-zone size evolution shown in Fig. 5 is independent of the details of the reionization model. The two cases shown in Fig. 5 have overlap redshifts for the mean IGM at $z = 6.2$ (with $\Delta_c = 20$) and $z = 7$ (with $\Delta_c = 5$). The corresponding ionization rate as a function of redshift for these models is shown in the upper left-hand panel of Fig. 5. While the evolution of the near-zone sizes can be successfully reproduced using an evolution for the ionization rate predicted by our model at the tail-end of the overlap phase, the near-zone sizes themselves cannot not be used as a probe of this process. This is because the rapid evolution in the near-zone sizes is attributable to a relatively small change in the IGM effective optical depth, and therefore is no more sensitive to the re-ionization history than the GP trough. It is nevertheless gratifying that we can qualitatively reproduce the evolution of the near-zone sizes with our analytical model, which is calibrated with the evolution of the background ionization rate measured from the effective optical depth in typical regions of the spectra. Note, however, that our analytic model is likely to overestimate the near-zone size both because it does not account for attenuation of quasar flux due to intervening neutral clumps in the IGM, and because the near-zone size is computed for average absorption properties in a clumpy IGM. Full numerical modelling with radiative transfer is required to reliably interpret the spectra of individual high-redshift quasars. We present such numerical simulations in the next section.

5 MODELLING THE OBSERVED NEAR-ZONE SIZE EVOLUTION WITH RADIATIVE TRANSFER SIMULATIONS

We now combine our semi-analytical model for the ionization rate in the biased regions surrounding quasars with a radiative transfer implementation and realistic density distributions drawn from a large cosmological hydrodynamical simulation. These simulations have been discussed in detail in Bolton & Haehnelt (2007a), and their description is not reproduced here. However, we have made three important changes. First, we include an evolving, density-dependent ionizing background using our semi-analytic model, which has been calibrated to observations at lower redshift. This addition is important because we have argued that it is the increase in the intensity of the ionizing background which leads to the rapid increase observed in the quasar near-zone sizes at $z < 6$. Secondly, we construct the absorption spectra using an ionizing background computed as a function of proper time along the trajectory of a photon emitted by the quasar, rather than at the proper time of the quasar. This effect is appropriate when considering spectra at the end of the reionization era, when the ionizing background can evolve significantly during the light travel time across a quasar near-zone. Thirdly, we have increased the temperature in the surrounding IGM within 15 proper Mpc of the quasar to $\sim$40 000 K to take into account the possibility that the hydrogen and helium in the near-zone have been highly ionized by a hard spectrum. We will discuss this point in more detail below.

In Fig. 7, we show the synthetic quasar absorption spectra used in this study. The redshifts and luminosities correspond to the 16 quasars analysed in the sample of Fan et al. (2006), plus the two additional quasars reported recently by Willott et al. (2007). The

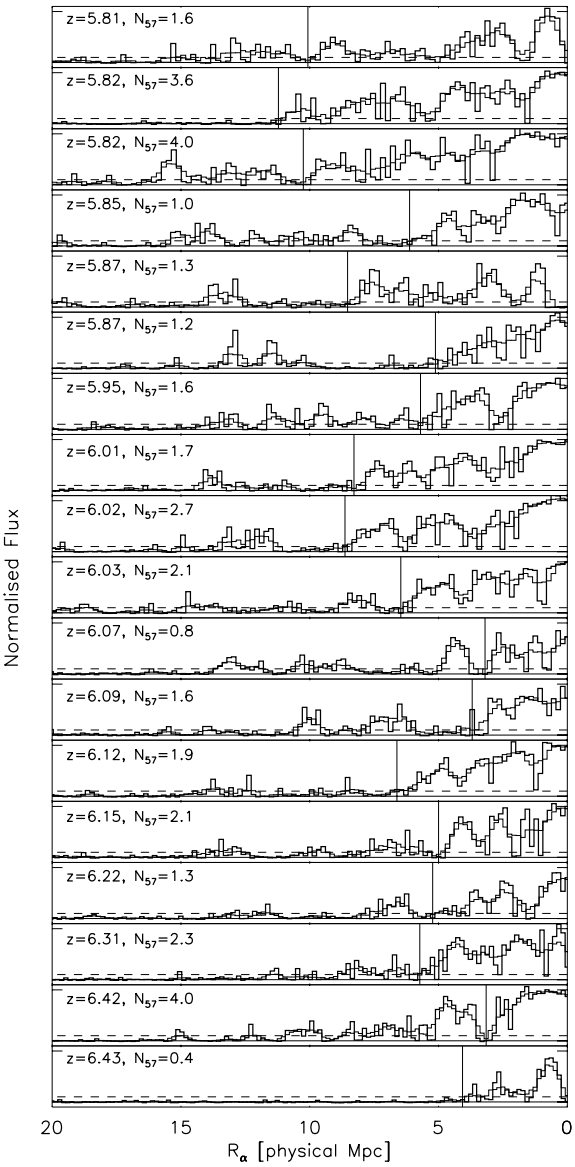

Figure 7. Synthetic Echelle Spectrograph and Imager (ESI) spectra of high-redshift quasar near-zones. The thick solid lines show the spectra at the computed resolution and the thin solid lines show the spectra smoothed by a top-hat filter of width 20 Å bins to allow comparison with observational data. The vertical lines mark the measured near-zone size using the definition of Fan et al. (2006).

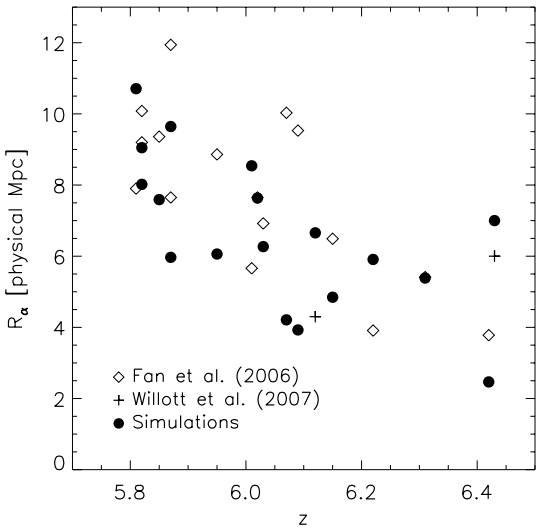

Figure 8. The near-zone sizes measured from synthetic spectra, plotted as a function of redshift (filled circles), along with the observational data of Fan et al. (2006) (open diamonds) and Willott et al. (2007) (crosses). The temperature in the surrounding IGM within 15 proper Mpc of the quasar has been raised to ∼40 000 K to take account of the possibility that the helium in the near-zone has been highly ionized by a hard spectrum.

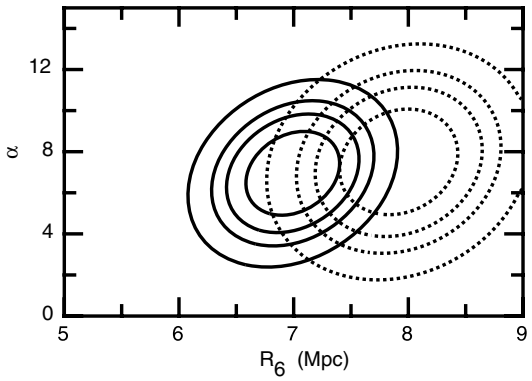

Figure 9. Constraints on the parameters α and R_6 that describe the evolution of model near-zone sizes with redshift. The model had $\dot{N} = 2 \times 10^{57}\,\mathrm{s}^{-1}$ and a large IGM temperature within 15 Mpc of the quasar. In each case, the extrema of the contours presented represent the 68, 84, 91 and 97 per cent bounds on single parameters. The observational constraints assuming a scaling of $L^{1/2}$ are reproduced (dotted contours).

emission rate of ionizing photons by the quasars, $\dot{N}$, is displayed in each panel of Fig. 7, normalized by $10^{57}\,\mathrm{s}^{-1}$. The thick solid lines show the synthetic spectra after processing them to resemble data obtained with the Keck telescope Echelle Spectrograph and Imager [see Bolton & Haehnelt 2007a for details], while the underlying thin solid lines show these spectra after smoothing by a top-hat filter of width of 20 Å. The vertical lines mark the locations of the near-zone sizes as defined by Fan et al. (2006), where the smoothed spectrum first drops below a transmission threshold of 10 per cent. The spectra clearly show the suppression of flux bluewards of the Lyα line, and the gradual appearance of an Lyα forest towards lower redshifts. The use of an evolving ionization rate calculated at the proper time along the observed line-of-sight is necessary to consistently model this progression.

The sizes of the near-zones derived from the 18 synthetic spectra are plotted as a function of redshift in Fig. 8 (filled circles) along with the observational data from Fan et al. (2006) (open diamonds) and Willott et al. (2007) (crosses). Following Fan et al. (2006), the sizes have been rescaled to a common AB magnitude of $M_{1450} = -27$ by assuming that the near-zone size is proportional to $\dot{N}^{1/3}$. There is very good agreement between the observed and simulated samples of spectra. We have performed the χ^2 minimization on the parametrized evolution for the sample of 18 simulated near-zones, with the resulting constraints plotted in Fig. 9.

We find parameters describing the mean relation of $R_6 = 7.0 \pm 0.4$ and $\alpha = 6.9 \pm 2$. The intrinsic scatter is at a level of ± 1.2 Mpc. These near-zones are slightly smaller than those observed. The modelled near-zones show an evolution that is consistent with the observed rate of evolution. However, as we found for the observed near-zones, the models are not consistent with evolution due to IGM density alone ($\alpha = 2$). The scatter of model near-zone sizes is consistent with the scatter among the observed near-zone sizes. Note, however, that any scatter due to expected variations in the quasar emission histories and the subsequent impact on the IGM has been neglected in the simulations.

We now return to the discussion regarding the temperature of the IGM we adopted when constructing the synthetic near-zone spectra. When computing $\dot{N}$, each quasar is assumed to have a broken power-law SED similar to that reported by Telfer et al. (2002):

$$\epsilon_\nu \propto \nu^{-0.5} \ \text{for} \ 1050 < \lambda < 1450\,\text{Å},$$
$$\propto \nu^{-1.5} \ \text{for} \ \lambda < 1050\,\text{Å}. \quad (23)$$

Thus, $M_{1450} = -27$ corresponds to $\dot{N} = 1.9 \times 10^{57}\,\mathrm{s}^{-1}$, and the 18 quasars in the Fan et al. (2006) and Willott et al. (2007) samples span a range of $0.4 < \dot{N}/10^{57}\,\mathrm{s}^{-1} < 4.0$. In Bolton & Haehnelt (2007a), it was noted that, even with a suitable increase in the ionizing background towards lower redshift, these quasar luminosities appeared to be too low to reproduce the absolute sizes of the observed near-zones with the simulations when using the definition advocated by Fan et al. (2006), particularly at $z < 6$ where the near-zone sizes are increased by the additional transmission from the emerging Lyα forest.

Consequently, in order to reproduce the observational result of Fan et al. (2006), each quasar in the simulations of Bolton & Haehnelt (2007a) also had a value of $\dot{N}$ which was increased by a factor of 2.5 relative to the value corresponding to $M_{1450} = -27$ for our adopted SED. Since a factor of 2.5 increase in the quasar luminosity is rather large, it was argued that this increase may be instead attributable to the increased mean-free-path for ionizing photons in the near-zone, which leads to an enhanced contribution from the ionizing background due to galaxies. In this work, we have consistently modelled the ionizing background due to galaxies by including the effect of reionization bias in the near-zone in detail. Nevertheless, we find the enhancement of the ionization rate in the near-zone due to this effect alone is still not enough to resolve this difference in the simulations. Note that this is not in contradiction with our analytical model predictions for the near-zone sizes. As stressed previously, the analytical estimates are likely to overestimate the near-zone sizes. We have therefore re-examined the assumptions which go into our numerical modelling.

In the case of a classical proximity zone, the neutral hydrogen fraction and thus the sizes of the near-zones do not only depend on the ionization rate but are also rather sensitive to the temperature of the IGM in the near-zone. This is due to the temperature dependence of the recombination rate for ionized hydrogen; in ionization equilibrium the neutral hydrogen density $n_{\rm HI} \propto T^{-0.7}/\Gamma_{12}$. Therefore, a

factor of 2.5 increase in the ionization rate is equivalent to around a factor of 4 increase in the ambient IGM temperature. In Bolton & Haehnelt (2007a), the numerical simulations had a median IGM temperature of $\sim$15 000 K before the quasar turned on, with the gas assumed to be in ionization equilibrium with the ionizing background. However, since the cooling time-scale for the low-density IGM is typically of the order of a Hubble time at $z = 6$, changes in the gas temperature made during a putative earlier accretion phase by the quasar would still persist. For example, if the quasar reionized the hydrogen and helium around it during an earlier phase when it had a very hard spectral index and the IGM was largely neutral, radiative transfer effects can increase the temperature in the IGM to $\sim$30 000–40 000 K (Abel & Haehnelt 1999; Bolton, Meiksin & White 2004; Tittley & Meiksin 2006). The IGM will then have only cooled marginally during the interval between active quasar phases. Although our radiative transfer scheme does correctly include these kind of effects, the heating boost is not present in our current simulations. This is because we assume that the IGM is already highly ionized by our model ionizing background before the quasar turns on, and we do not model the previous emission history of the quasar, which would require substantially more detailed simulations.

Therefore, to mimic this effect, we have raised the temperature in our simulations within 15 Mpc of the quasar by a factor of 2.5, corresponding to a median value of $\sim$40 000 K. Note that this temperature is smaller than the value of $\sim$60 000 K one would expect based according to the scaling relation discussed above, which is higher than can be easily achieved by photoionization. Nevertheless the near-zone sizes are in good agreement with that of the observed sample. The deviation from the expected scaling is due to the reionization bias which we had not taken into account in Bolton & Haehnelt (2007a). Our model for the increased ionizing background in the biased regions surrounding quasars helps to increase the near-zone sizes and drive their rapid evolution. As discussed above, our simulations provide a good description of the observed near-zone sizes with the observed luminosities and reasonable assumptions for the quasar SED, and may thus provide a hint that the IGM is substantially hotter than average around the highest-redshift quasars.

There remains a small discrepancy between observed and modelled near-zone sizes (Fig. 9). However, as already mentioned we have not modelled the effect of the quasar radiation on the mean-free-path in the near-zone. There is also the possibility that the discrepancy is partially due to a continuum on the observed spectra which has been placed too low, or perhaps a quasar SED which is different from the one we have assumed. Considering these uncertainties, the agreement appears excellent.

In summary, our semi-analytic modelling of the history for the ionizing background, combined with numerical simulation of the Lyα transmission in quasar near-zones, is able to quantitatively describe the evolution of quasar near-zone sizes at $6.4 < z < 5.8$, and the evolution of the ionizing background at $z \sim 4$–6. We find that the rapid evolution observed in the sizes of the high-redshift quasar near-zones is due to the increasing level of ionizing background near $z \sim 6$, with absolute sizes which suggest an increased IGM temperature in the vicinity of the quasars.

6 SUMMARY AND CONCLUSIONS

Absorption spectra of high-redshift quasars show an increasingly thick Lyα forest, suggesting an increase in the fraction of neutral gas in the IGM approaching $z \sim 6$, culminating in the complete lack of detected flux in the GP trough bluewards of the Lyα line. However, the meaning of the complete GP troughs remains controversial, having been interpreted both as the completion of the reionization epoch, and as merely a gradual thickening of the Lyα forest. The inconclusive nature of the observations has its root in the very large cross-section for absorption of Lyα photons, which allow a direct probe of the neutral hydrogen content of the IGM only down to volume-averaged neutral fractions of around 10^{-4}.

The fact that quasars reside in massive haloes places them in overdense and strongly biased regions of the IGM. This presents an additional challenge for the interpretation of regions in quasar absorption spectra close to the quasars intrinsic redshift, since one is using results from these biased regions to infer the properties of the mean IGM. In this work, we have presented a model for the evolution of the emissivity of ionizing photons and the ionization state of the IGM that takes such a reionization bias in the environment of bright, high-redshift quasars into account. In our CDM-based model, the ionizing photons for reionization are produced by star formation in dark matter haloes spanning a wide mass range. At redshifts both prior to, and post-overlap, our model allows us to calculate values for the volume- and mass-averaged neutral fractions, the ionizing photon mean-free-path and the evolution of the ionizing background. With appropriate choices for the parameters controlling the star formation efficiency, we are able to reproduce the ionizing emissivity at $4 < z < 6$ and the ionizing photon mean-free-path at $z \sim 4$ inferred from the observed opacity distribution in Lyα forest absorption spectra. In our model, the comoving ionizing emissivity is roughly constant with redshift and the volume filling factor of ionizing regions increases slowly from 10 to 90 per cent between $z \gtrsim 10$ and $z \sim 6$–7, where reionization completes following the overlap of cosmological H II regions. Within 5 physical Mpc of a high-redshift quasar, we find that the evolution of the ionization state of the IGM precedes that of the mean universe by around 0.3 redshift units. During the period shortly after overlap, the mean-free-path is seen to increase rapidly in the model. The offset in the redshift of overlap between overdense regions and the mean IGM therefore results in an ionizing background near high-redshift quasars (excluding the flux of ionizing radiation from the quasar itself) that exceeds the value in the mean IGM by a factor of $\sim$2–3 for a short period of time.

High-redshift quasar spectra also show evidence for a highly ionized region immediately surrounding the quasar. Using our semi-analytic prescription for biased reionization, we model the evolution of these quasar near-zones. We find near-zone sizes which exhibit a redshift dependence which is qualitatively consistent with the current observational data. The model indicates that the rapid evolution in the near-zone sizes in the redshift range $5.8 < z < 6.4$ is due to the increasing background ionization rate originating from an almost constant galactic emissivity. Within our model, this rise in the background ionization rate is therefore due to the rapid rise in the mean-free-path for ionizing photons, which is expected near the tail-end of the reionization epoch as H II regions overlap. We note that our model generates an optical depth to Thomson scattering for CMB photons of $\tau_{\rm es} = 0.45$, which is smaller than the values determined from the *WMAP* satellite (Spergel et al. 2007). Models which include the possible effect of massive Population III stars partially reionize the IGM at higher redshifts and result in larger values of $\tau_{\rm es}$ (e.g. Choudhury & Ferrara 2006; Wyithe & Cen 2007). We have not included Population III stars in our modelling. However, we have argued that the rapid evolution in quasar near-zone sizes arises due to the rapid evolution of the mean-free-path at the tail end of the overlap era. As a result our conclusions will not be sensitive to partial reionization at high redshifts prior to the overlap era.

In order to model the opacity distribution in spectra of bright high-redshift quasars in more detail, we have combined our model for the evolution of the metagalactic ionization rate in the biased environment surrounding quasars with detailed line-of-sight radiative transfer simulations in the inhomogeneous high-redshift IGM. In this way, we were able to reproduce the sizes of the observed near-zones and their rapid evolution in the redshift range $5.8 < z < 6.4$ very well. Our numerical modelling also suggests that the rapid evolution is not due directly to large changes in the neutral hydrogen fraction of the mean IGM, with a simple scaling between neutral fraction and near-zone size. Instead, as suggested by Bolton & Haehnelt (2007a), the near-zone sizes probe the evolution of the background ionization rate, which results in modest changes to an already very small neutral fraction. We furthermore find that the absolute sizes of the near-zones are rather sensitive to the IGM temperature in the near-zones, due to the temperature dependence of the recombination rate. The observed near-zone sizes are reproduced, given the observed quasar ionizing luminosities if the temperature of the surrounding IGM is high ($\sim$40 000 K). Heating to such high temperatures at distances of up to 10–15 proper Mpc may be plausible if the hydrogen and helium in the near-zone have been highly ionized by a hard spectrum prior to the completion of reionization in the IGM as a whole. This requires the continuous or intermittent emission of a hard spectrum for an extended period of time. If the IGM temperature is not as hot as 40 000 K, the differences found between modelled and observed near-zone sizes could be explained as at least partially being due to a continuum on the observed spectra which has been placed too low, or perhaps a quasar SED which is different from the one we have assumed.

There are still several issues to address regarding the sizes and redshift evolution of high-redshift quasar near-zones. Larger samples will clarify the significance of the evolution observed in the present data and hopefully constrain the evolution at even higher redshift. A more detailed modelling of the quasar accretion history and the ensuing flux of ionizing photons may be required to self-consistently model near-zone sizes. The detection of strongly broadened absorption lines within quasar near-zones would lend support to a scenario in which IGM temperatures within quasar near-zones are increased by the reionization of hydrogen and helium by a hard spectrum. However, in this work we have presented a simple reionization model with a roughly constant ionizing emissivity, in which reionization ends following a rapid increase in the ionizing photon mean-free-path as H II regions overlap at $z \sim 6$–7. This scenario successfully reproduces the gross features present in high-redshift quasar absorption spectra, both within and outside the quasar near-zones.

ACKNOWLEDGMENTS

This work was supported in part by the Australian Research Council. JSBW acknowledges the hospitality of the Institute of Astronomy at the Cambridge University where part of this work was undertaken.

REFERENCES

Abel T., Haehnelt M. G., 1999, ApJ, 520, L13
Alvarez M. A., Abel T., 2007, MNRAS, 380, L30
Bardeen J. M., Bond J. R., Kaiser N., Szalay A. S., 1986, ApJ, 304, 15
Barkana R., Loeb A., 2001, Phys. Rep., 349, 125
Becker G. D., Rauch M., Sargent W. L. W., 2007, ApJ, 662, 72
Bolton J. S., Haehnelt M. G., 2007a, MNRAS, 374, 493
Bolton J. S., Haehnelt M. G., 2007b, MNRAS, 381, L35
Bolton J., Meiksin A., White M., 2004, MNRAS, 348, L43
Bond J. R., Cole S., Efstathiou G., Kaiser N., 1991, ApJ, 379, 440
Cen R., Haiman Z., 2000, ApJ, 542, L75
Choudhury T. R., Ferrara A., 2005, MNRAS, 361, 577
Choudhury T. R., Ferrara A., 2006, MNRAS, 371, L55
Ciardi B., Ferrara A., 2005, Space Sci. Rev., 116, 625
Dijkstra M., Haiman Z., Rees M. J., Weinberg D. H., 2004, ApJ, 601, 666
Efstathiou G., 1992, MNRAS, 256, 43
Fan X. et al., 2006, AJ, 132, 117
Faucher-Giguere C.-A., Lidz A., Zaldarriaga M., Hernquist L., 2007, ApJ, submitted (astro-ph/0701042)
Fukugita M., Hogan C. J., Peebles P. J. E., 1998, ApJ, 503, 518
Furlanetto S. R., Zaldarriaga M., Hernquist L., 2004, ApJ, 613, 16
Gnedin N. Y., 2000, ApJ, 535, 530
Gnedin N. Y., Fan X., 2006, ApJ, 648, 1
Gnedin N. Y., Kravtsov A. V., Chen H.-W., 2007, preprint, 707 (arXiv:0707.0879)
Guimarães R., Petitjean P., Rollinde E., de Carvalho R. R., Djorgovski S. G., Srianand R., Aghaee A., Castro S., 2007, MNRAS, 377, 657
Leitherer C. et al., 1999, ApJS, 123, 3
Lidz A., McQuinn M., Zaldarriaga M., Hernquist L., Dutta S., 2007, ApJ, submitted (astro-ph/0703667)
Madau P., Rees M. J., 2000, ApJ, 542, L69
Maselli A., Gallerani S., Ferrara A., Choudhury T. R., 2007, MNRAS, 376, L34
Mesinger A., Haiman Z., 2004, ApJ, 611, L69
Miralda-Escudé J., Haehnelt M., Rees M. J., 2000, ApJ, 530, 1
Mo H. J., White S. D. M., 1996, MNRAS, 282, 347
Press W., Schechter P., 1974, ApJ, 187, 425
Sheth R., Tormen G., 2002, MNRAS, 321, 61
Sheth R. K., Mo H. J., Tormen G., 2001, MNRAS, 323, 1
Songaila A., 2004, AJ, 127, 2598
Spergel D. N. et al., 2007, ApJS, 170, 377
Srbinovsky J. A., Wyithe J. S. B., 2007, MNRAS, 374, 627
Telfer R. C., Zheng W., Kriss G. A., Davidsen A. F., 2002, ApJ, 565, 773
Thoul A. A., Weinberg D. H., 1996, ApJ, 465, 608
Tittley E. R., Meiksin A., 2006, MNRAS, 380, 1369
White R., Becker R., Fan X., Strauss M., 2003, AJ, 126, 1
Willott C. J. et al., 2007, preprint, 706 (arXiv:0706.0914)
Wyithe J. S. B., Cen R., 2007, ApJ, 659, 890
Wyithe J. S. B., Loeb A., 2003, ApJ, 586, 693
Wyithe J. S. B., Loeb A., 2004, Nat, 427, 815
Wyithe J. S. B., Loeb A., Carilli C., 2005, ApJ, 628, 575

This paper has been typeset from a TEX/LATEX file prepared by the author.